Coupling growth-factor engineering with nanotechnology for therapeutic angiogenesis

Rituparna Sinha Roy[a,b], Shivani Soni[a,b], Rania Harfouche[a,b], Pooja R. Vasudevan[c], Oliver Holmes[d], Hugo de Jonge[d], Arthur Rowe[d], Abhimanyu Paraskar[a,b], Dirk M. Hentschel[a], Dimitri Chirgadze[f], Tom L. Blundell[f], Ermanno Gherardi[d,1], Raghunath A. Mashelkar[b,e,1], and Shiladitya Sengupta[a,b,1]

[a]Department of Medicine, Brigham and Women's Hospital, Harvard Medical School, Boston, MA 02115; [b]Harvard-Massachusetts Institute of Technology (MIT) Division of Health Sciences and Technology, Cambridge, MA; [c]Massachusetts Institute of Technology, Cambridge, MA; [d]Medical Research Council MRC Center, Cambridge CB2 2QH, United Kingdom; [e]National Chemical Laboratory, Pune, 411008, India; and [f]Department of Biochemistry, University of Cambridge, 80 Tennis Court Road, Cambridge CB2 1GA, England

Contributed by Raghunath A. Mashelkar, May 3, 2010 (sent for review February 27, 2010)

Therapeutic angiogenesis is an emerging paradigm for the management of ischemic pathologies. Proangiogenic Therapy is limited, however, by the current inability to deliver angiogenic factors in a sustained manner at the site of pathology. In this study, we investigated a unique nonglycosylated active fragment of hepatocyte growth factor/scatter factor, 1K1, which acts as a potent angiogenic agent in vitro and in a zebrafish embryo and a murine matrigel implant model. Furthermore, we demonstrate that nanoformulating 1K1 for sustained release temporally alters downstream signaling through the mitogen activated protein kinase pathway, and amplifies the angiogenic outcome. Merging protein engineering and nanotechnology offers exciting possibilities for the treatment of ischemic disease, and furthermore allows the selective targeting of downstream signaling pathways, which translates into discrete phenotypes.

HGF/SF | protein engineering | ischemic disease | cardiovascular disease | nanoparticle

Neovascularization in the adult holds the potential for ameliorating ischemic disease, which is the leading cause of morbidity and mortality in the United States (1). Ferrara and Kerbel recently articulated that "*therapeutic angiogenesis*" is an emerging and exciting frontier of cardiovascular medicine (2). However, while early preclinical studies and phase I clinical trials exhibited promising results with recombinant proteins or gene therapy, more rigorous phase II and III studies have reported conflicting outcomes (3–6). A recent review of these clinical trials highlighted vector "washout" leading to inadequate duration of exposure to the angiogenic agent as a key factor that may have impaired the effectiveness of therapy (7). Indeed, it is now established that sustained activation of downstream signal pathways promotes cellular processes critical for angiogenesis (8). We rationalized that harnessing a nanotechnology-based approach can enable a temporal control over the presentation of the angiogenic factors to the cellular target, thereby altering the activation of downstream signal transduction.

While nanoformulation of angiogenic proteins is an attractive strategy, the synthesis and instability of these large complex glycosylated structures pose a significant barrier (9). Hepatocyte growth factor/scatter factor (HGF/SF) is a potent angiogenic agent (10), signaling through the Met receptor and downstream MAPK and the PI3K pathways (11–12). Interestingly, the Met receptor is upregulated during hypoxia, suggesting that the ischemic tissue will be primed for activation by HGF/SF (13). These results indicate that HGF/SF could emerge as an attractive therapy for angiogenesis. However, HGF/SF is a heparin-binding protein with a complex multidomain structure consisting of an N-terminal (N) domain, four copies of the kringle domain (K1 to K4) and a C-terminal domain homologous to that of serine proteineases (SP) (Fig. 1*A*) (14). Biologically active HGF/SF is produced by proteolytic cleavage of the linker connecting the fourth kringle and the SP domain yielding a two-chain (α/β)-heterodimer, in which both the α- and the β-chain display considerable heterogeneity due to five putative glycosylation sites: three in the α-chain (residues 289, 397, and 471) and two in the β-chain (residues 561 and 648).

In the present study, we combined protein engineering and nanotechnology in order to maximize the therapeutic potential of HGF/SF. The protein engineering experiments targeted NK1, an alternatively spliced variant of the HGF/SF transcript to yield the protein 1K1, a stable and nonglycosylated agonist of the Met receptor, which exerted strong angiogenic activity. Furthermore we encapsulated 1K1 in nanoparticles engineered from biodegradable D, L-lactic acid-co-glycolic acid copolymer to enable sustained release, and demonstrate that the temporal release enables unique downstream signaling through the MAPK pathway resulting in an enhanced angiogenic outcome in vitro and in vivo. Our study opens up the possibility of combining unique approaches to protein engineering and nanovectors for modulating vascularization in impaired ischemic condition.

Results and Discussion

Engineering 1K1, a Nonglycosylated HGF/SF Variant. In the presence of heparan sulfate or heparin, NK1 behaves as a partial receptor agonist (14). In order to develop 1K1, a rational protein engineering approach was employed based on structural and functional studies of NK1 (15), NK1-heparin complexes (16), and individual N and K1 domains (17). NK1 binds heparin through two distinct sites: a high-affinity site located in the N domain and formed by the side chains of R73, K60, T61, R76, K62, and K58 and main chain atoms of T61, K63, and G79 (18) and a low-affinity site in the K1 domain comprising the side chains of K132, R134, K170, and R181. The mutant 1K1 carries two reverse charge mutations at K132 and R134 (1K1: K132E:R134E) that disrupt heparin binding to the kringle domain (Fig. 1) and displays increased signaling activity on several cell types compared to wild type (16). The higher biological activity of 1K1 over NK1 is due to two reasons: Firstly, as a result of the loss of the heparin-binding site in K1, heparin interacts solely with the primary binding site in the N domain and causes adjacent 1K1 dimers to bind Hepatocyte

Author contributions: R.S.R., S.S.(Soni), R.H., O.H., H.d.J., A.R., A.P., D.M.H., E.G., R.A.M., and S.S.(Sengupta) designed research; R.S.R., S.S.(Soni), R.H., P.R.V., O.H., H.d.J., A.R., A.P., and E.G. performed research; O.H., H.d.J., A.R., D.M.H., and E.G. contributed new reagents/analytic tools; R.S.R., S.S.(Soni), R.H., P.R.V., O.H., H.d.J., A.R., D.M.H., E.G., and S.S.(Sengupta) analyzed data; and R.S.R., S.S.(Soni), R.H., E.G., R.A.M., and S.S.(Sengupta) wrote the paper.

The authors declare no conflict of interest.

Data deposition: The atomic coordinates and structure factors have been deposited in the Protein Data Bank, www.pdb.org (PDB ID code 3MPK).

[1]To whom correspondence may be addressed: E-mail: ram@ncl.res.in, egherard@mrc-lmb.cam.ac.uk, or shiladit@mit.edu.

This article contains supporting information online at www.pnas.org/lookup/suppl/doi:10.1073/pnas.1006007107/-/DCSupplemental.

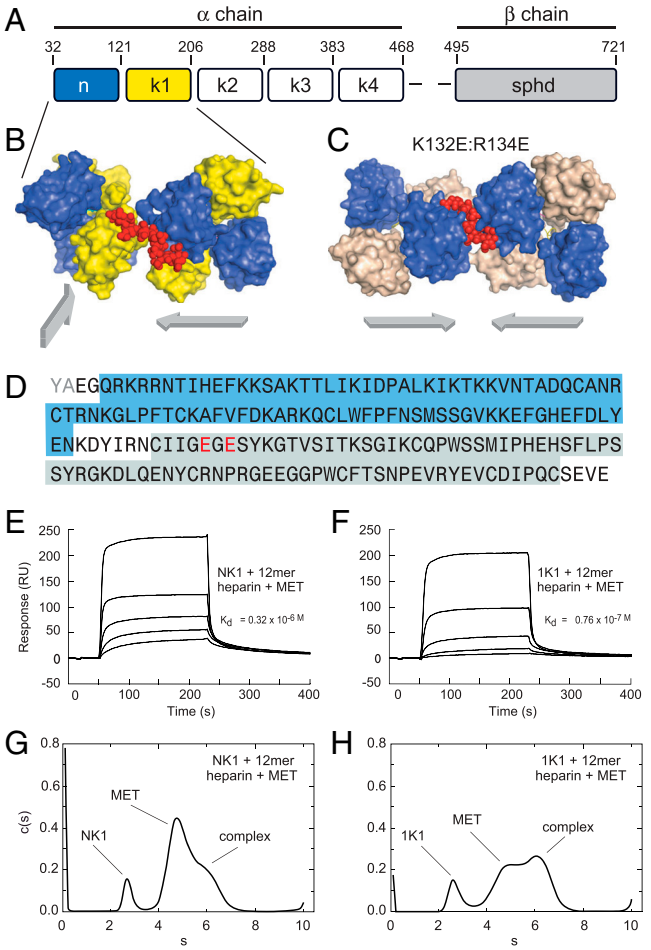

Fig. 1. Structural features of the 1K1-heparin complex and interaction with the MET receptor (*A*) Domain structure of full length multidomain HGF/SF. The α-chain consists of N-terminal domain (amino acids 32–121) and four kringle domains(K1, K2, K3, and K4) and the β-chain contains serine protinease domain (spdh domain). (*B*) Crystal structure of NK1-heparin complex (16) (PDB accession 1GMO). Two NK1 dimers are shown bridged by heparin. N and K domains are shown in *blue* and *yellow*, heparin is shown in *red* (*C*) Crystal structure of 1K1-heparin complex (PDB accession 3MPK). Two 1K1 dimers are shown bridged by heparin. N and K domains are shown in *blue* and *gray*, heparin is shown in *red*. The figures in *B* and *C* have been drawn with Pymol. Reverse mutations K132E and R134E were introduced into K1 domain of 1K1 to inactivate the low-affinity heparin-binding sites. (*D*) and (*E*). (*D*) Amino acid sequence of 1K1 demonstrating the mutated sites. Binding of NK1 (*E*) and 1K1 (*F*) to MET567 in the presence of 12mer heparin using surface plasmon resonance. Twofold dilutions of each protein were used from a concentration of top concentration of 200 nM. The concentration of 12mer heparin in the sample and in the reaction buffer was 10 μM. (*G*) and (*H*). Velocity sedimentation analysis of ternary complexes of NK1-heparin-MET567 (*G*) and 1K1-heparin-MET567 (*H*). Data show plots of c(s) against s*20,w. In the presence of 10mer heparin, the amount of ternary complex is significantly higher for 1K1 than for NK1.

growth factor receptor (MNNG (N-Methyl-N'-nitro-Nnitrosoguanidine) HOS Tranforming gene) (MET) on the same plane (Fig. 1*C*) unlike NK1, where the heparin-binding sites of the K1 domain cause heparin to align adjacent NK1 dimers on a different plane (Fig. 1*B*). Hence, 1K1 can form oligomeric ligand-receptor complexes more readily than NK1. (*A full description of the crystal structure of the 1k1-heparin complex will be reported elsewhere.*) Secondly, preformed 1K1-heparin complexes have greater binding affinity for MET than NK1- heparin complexes as a result of the different way in which the two proteins bind heparin as shown by surface plasmon resonance (Fig. 1 *E–F*) and velocity and sedimentation experiments (Fig. 1 *G–H*).

1K1 Induces Angiogenesis in Vitro by Binding to MET Kinase. The angiogenic phenotype is the culmination of discrete cellular steps characterized by endothelial cell chemoinvasion, proliferation, and tubulogenesis (18). As shown in Fig. S1, both HGF/SF and 1K1 induced endothelial cell proliferation. Furthermore, 1K1-induced endothelial cell proliferation was inhibited by the MET kinase inhibitor, PHA 665752, in a concentration-dependent manner (Fig. S1*C*), which confirmed that 1K1 induces angiogenesis through the Met receptor. Previous studies have revealed that MET binding by HGF/SF ligand results in downstream signaling through the PI3K and the MAPK (10). To test whether these pathways are activated in 1K1-mediated endothelial cell proliferation, we pretreated the cells with LY294002 or PD98059, which inhibit PI3K and MAPK respectively. As shown in Fig. S1, both LY294002 and PD98059 inhibited 1K1-induced

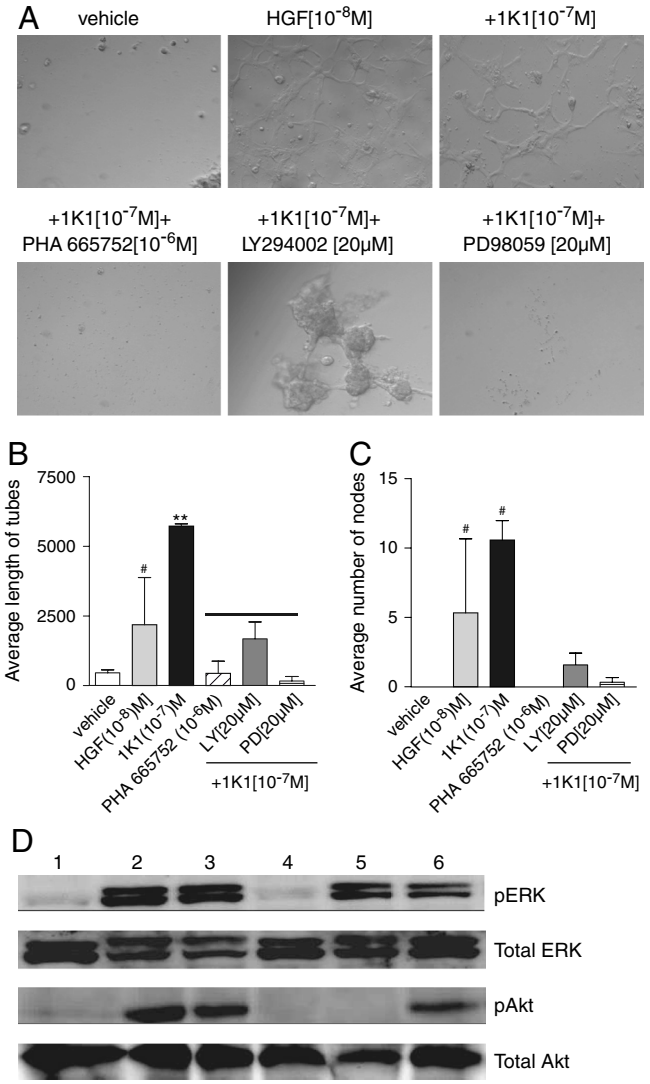

Fig. 2. (*A*) Effect of pharmacological inhibitors on the 1K1-induced on HUVECs tube formation on growth-factor-reduced matrigel. Graphs (*B*) and (*C*) show the quantification of the images using three morphometric analyses of average length of tubes and average number of nodes respectively. The data represent mean ± SEM pixels from $n = 3$. ** $P < 0.01$ vs. vehicle-treated control; # $P < 0.05$ vs. 1K1(10^{-7} M]). (*D*) Representative Western blot showing phospho Erk and total Erk and also phospho Akt and total Akt expression in HUVECs treated with Met inhibitor PHA 665752 (10^{-6} M), LY294002 (50 μM) and PD98059 (50 μM) for 2 h, followed by 1K1 for 10 mins. The numbers indicate **1:** vehicle, **2:** HGF/SF (10^{-8} M), **3:** 1K1 (10^{-7} M), **4:** 1K1 + PHA 665752 (10^{-6} M) **5:** 1K1 + LY294002 (50 μM), **6:** 1K1 + PD98059 (50 μM). For sample no. 4, 5, and 6, **1K1** (10^{-7} M) were used along with the inhibitors.

cell proliferation in a concentration-dependent manner, suggesting that both the PI3K and MAPK pathways are implicated during 1K1-induced endothelial cell proliferation.

We next tested whether 1K1 can induce endothelial tubulogenesis. As shown in Fig. 2, both HGF/SF and 1K1 induced significant tubulogenesis compared with vehicle treatment when the endothelial cells were plated on a three-dimensional Matrigel matrix. Interestingly, 1K1-induced tubes were phenotypically longer and had more nodes as compared with HGF/SF. Consistent with the cell proliferation results, pretreatment of the human umbilical vein endothelial cells (HUVECs) with 10^{-6} M PHA665752 completely blocked 1K1-induced tubulogenesis (Fig. 2 *A–C*). Additionally, both PD98059 and LY294002 inhibited 1K1-induced tubulogenesis implicating these signaling pathways in the process (Fig. 2 *A–C*). Indeed, as seen in the Western blots (Fig. 2*D*), incubation of endothelial cells with 1K1 resulted in rapid phosphorylation of both ERK)and Akt, downstream effectors of the MAPK and PI3K signaling pathways, which were blocked by LY294002 and PD98059 respectively. Western blot also revealed that pretreating the cells with 10^{-6} M PHA665752 blocked the 1K1-induced phosphorylation of ERK and Akt. These results confirmed that 1K1 induces angiogenesis in vitro by signaling through the same Met-dependent pathways activated by HGF/SF (10).

Synthesis and Characterization of 1K1-Nanoparticle. A key challenge for therapeutic angiogenesis is the local and sustained delivery of the angiogenic factors at the desired site of action (6). In an elegant study, Richardson et al. demonstrated that sustained release of VEGF-165 and PDGF-BB, each with distinct kinetics, from a single, structural polymer scaffold resulted in the rapid formation of a mature vascular network (19). Furthermore, the controlled intramyocardial delivery of platelet-derived growth factor was found to improve postinfarction ventricular function with increased vascularization (20). Similarly, in a recent study, the intramuscular injection of pivastatin-loaded nanoparticles that enabled sustained release of the drug resulted in enhanced angiogenesis (21). To enable a sustained release formulation of 1K1, we engineered nanoparticles from poly-lactic acid-glycolic acid (PLGA) copolymer, which is biocompatible and biodegradable and is approved by the FDA. 1K1 nanoparticles were made using double emulsion/solvent extraction technique (22). Transmission electron microscopy data confirmed the spherical shape and also the diameter of the nanoparticles to be 60–140 nm (Fig. 3*A*), which was validated by dynamic light scattering measurement (Fig. 3*B*). The total loading efficiency of 1K1 in the nanoparticles, was determined to be $54.27 \pm 7.12\%$. Sustained release of therapeutic protein in biologically active form and subsequent degradation are critical for biologic activity, and depend on desorption of surface-bound molecules, diffusion through the nanoparticle matrix and erosion of the latter. Kinetics of 1K1 release from the nanoparticles over a 7 day period was determined by enzyme-linked immunoabsorbent assay. As shown in Fig. 3*C*, there was an initial phase of characteristic burst release associated with nanoparticles (22, 23) followed by a steady state release over a 7 day period. This observation is consistent with previous reports where VEGF entrapped in PLGA microsphere exhibited similar release kinetics over a 30 day period (22).

1K1-NP Induces Angiogenesis in Vitro. The angiogenic activity of 1K1-nanoparticles (1K1-NP) was examined using HUVECs proliferation as the biological read-out. As shown in Fig. 3 *D–F*, treatment with 1K1-NP resulted in significant endothelial cell proliferation as compared with vehicle, indicating that the process of engineering the nanoparticles does not alter the biological activity of 1K1. Furthermore, 1K1-NP-induced cell proliferation was inhibited in presence of MET inhibitor, PHA 665752 (Fig. 3*D*), the PI3K inhibitor, LY294002, (Fig. 3*E*), and the MAPK inhibitor, PD98059 (Fig. 3*F*), indicating that, following entrapment in the nanoparticle, signaling is mediated by the same pathways activated by soluble 1K1.

Interestingly, 1K1-NP was found to induce significantly greater tubulogenesis as compared with empty vector or free 1K1, indicating the sustained release of the angiogenic factor markedly affected the angiogenic response (Fig. 4). To mechanistically correlate the phenotypic distinctions with the temporal release, we used Western blotting to evaluate the effect of 1K1-NP on downstream signaling pathways. As shown in Fig. 4*C*, incubation of endothelial cells with both 1K1-NP and 1K1 resulted in rapid phosphorylation within 10 min. Pretreating the cells with PHA665752 blocked the phosphorylation of ERK and Akt induced by 1K1-NP. Pretreating the cells with 50 μM LY294002 abolished the phosphorylation of Akt while PD98059 reduced the phosphorylation of ERK consistent with 1K1 activity previously observed. However, in the case of 1K1-NP, a sustained activity was noted as shown by the increased phosphorylation of ERK at 8.5 h posttreatment unlike treatment with 1K1 (Fig. 4*D*). Indeed, it is now well established that sustained activa-

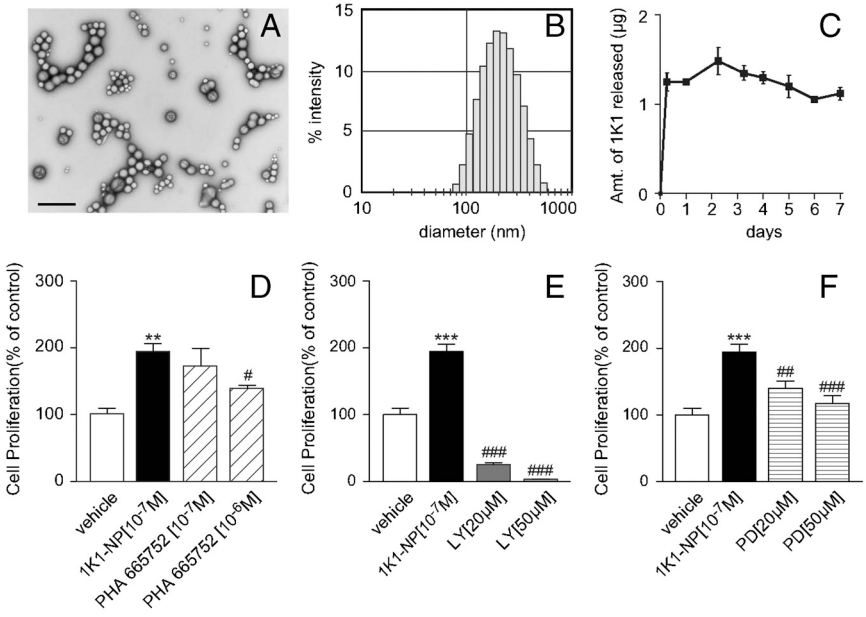

Fig. 3. (*A*) Transmission electron microscopy (TEM) image of 1K1-encapsulated nanoparticles (1K1-NP) (Bar = 500 nm). (*B*) Size distribution (in nm) of the 1K1-encapsulated nanoparticles by dynamic light scattering experiment. (*C*) Graph shows release kinetics of 1K1 from the nanoparticle when incubated in PBS at room temperature. The values on the Y-axis represent the amount of 1K1 released from the 1K1-NP in ug unit. (*D*) Effect of Met inhibitor, PHA 665752, on 1K1-NP induced HUVECs proliferation at 48 h. (*E*) Effect of PI3 kinase inhibitor, LY294002, on 1K1-NP induced HUVECs proliferation at 48 h. (*F*) Effect of MAP kinase inhibitor, PD98059, on 1K1-NP induced HUVECs proliferation at 48 h. The data represent mean ± SEM from $n = 3$. *** $P < 0.001$ vs. vehicle-treated control; ** $P < 0.01$ vs. vehicle-treated control; ### $P < 0.001$ vs. 1K1(10^{-7} M); ## $P < 0.01$ vs. 1K1(10^{-7} M); # $P < 0.05$ vs. 1K1(10^{-7} M).

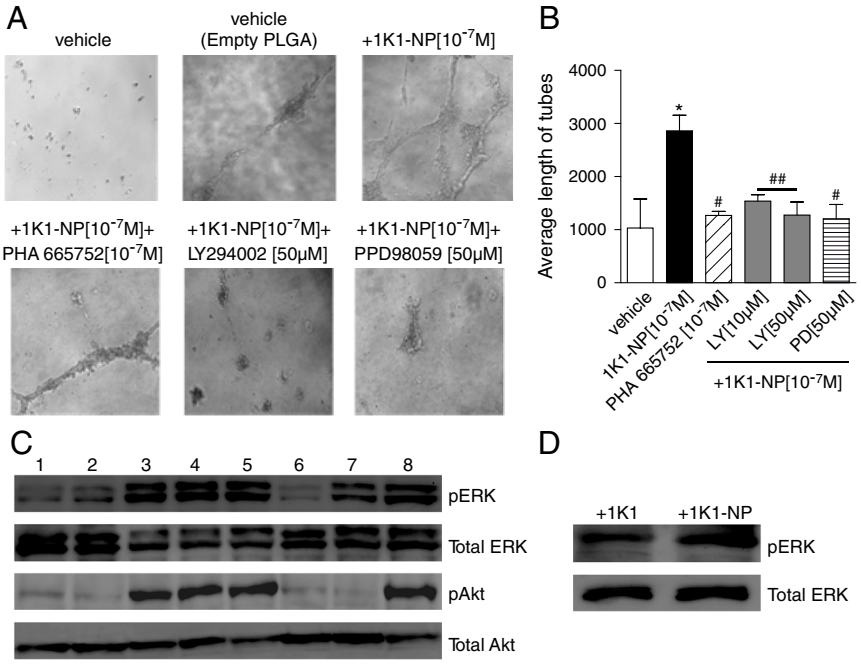

Fig. 4. (*A*) Effect of pharmacological inhibitors on the 1K1-NP induced on HUVECs tube formation on matrigel. (*B*) Graphs show the quantification of the images using average length of tubes. The data represent mean ± SEM pixels from $n = 3$. * $P < 0.05$ vs. vehicle-treated control; ## $P < 0.01$ vs. 1K1 (10^{-7} M); # $P < 0.05$ vs. 1K1(10^{-7} M). (*C*) Representative Western blot showing phospho Erk and total Erk and also phospho Akt and total Akt in HUVECs treated with Met inhibitor PHA 665752 (10^{-6} M), LY294002 (50 μM) and PD98059 (50 μM) for 2 h, followed by 10 min 1K1-NP and 1K1. The numbers indicate **1:** vehicle (PBS), **2:** vehicle (empty PLGA), **3:** freshly prepared 1K1 (0.5×10^{-7} M), **4:** 1K1 incubated at 37 °C for 24 h (0.5×10^{-7} M), **5:** 1K1-NP incubated at 37 °C for 24 h (0.5×10^{-7} M), **6:** 1K1-NP + PHA665752 (10^{-6} M)**7:** 1K1-NP + LY294002 (50 μM), **8:** 1K1-NP + PD98059 (50 μM). For sample no. 6, 7, and 8, (0.5×10^{-7} M) 1K1-NP were used along with the inhibitors. (*D*) Representative Western blot showing phospho Erk and total Erk in HUVECs treated with (0.5×10^{-7} M) 1K1 and (0.5×10^{-7} M) 1K1-NP for 8.5 h.

tion of MAPK signaling pathway is critical for tubulogenesis, whereas transient activation is insufficient to induce such morphological alterations (8, 24, 25). Phenotypic quantification of the vascular tubes also confirmed that pretreatment of the HUVECs with PHA665752 (10^{-7} M), PD98059 (50 μM) or LY294002 (50 μM) blocked 1K1-NP-induced tubulogenesis (Fig. 4 *A–B*).

Zebrafish Angiogenesis Assay. The zebrafish (*Danio rerio*) is fast emerging as an excellent model for studying neovascularization (26, 27). To validate the angiogenic activity of 1K1 and 1K1-NP in vivo, 1K1 or 1K1-NP were mixed with growth-factor-reduced matrigel (Mgel) and injected into the yolk sac, next to the subintestinal vessel. As shown in Fig. 5, 1K1 induced significant angiogenesis compared with empty vector as quantified by nodes formed during sprouting of the subintestinal vessels. Interestingly, at the 48 h time points, 1K1-NP exerted greater angiogenesis than 1K1, which validates the hypothesis that sustained release of angiogenic factors can result in enhanced angiogenesis.

Murine Matrigel Implant Assay. To further validate the angiogenic efficacy of 1K1 in vivo, 1K1 or 1K1-NP mixed with growth-factor-reduced matrigel was injected subcutaneously in mice at a dose of 200 nanogram (ng) of 1K1/scaffold. The scaffolds were maintained for 12 d, following which the animals were killed and the skin everted to visualize the angiogenic response. Treatment with 1K1 resulted in a strong angiogenic response as shown in Fig. 6. Interestingly, 1K1-NP induced a significantly greater angiogenic response as compared with 1K1. To further validate the gross morphology, the implants were cross-sectioned, immunolabeled for von Willebrand factor, a marker for endothelial cells. As shown in Fig. 6 (*lower*), 1K1-NP treatment (Fig. 6*H*) resulted in a superior angiogenic outcome to free 1K1, consistent with the observation in the zebrafish. These results confirm that sustained release of growth factors could exert superior angiogenic outcome.

Conclusions

While significant progress has been made towards inhibition of angiogenesis in a pathological context such as in cancer, therapeutic angiogenesis in diseases characterized by insufficient vascularization, such as in coronary ischemia, peripheral arterial diseases, or in diabetic sores (4, 28–30), is still at a nascent stage.

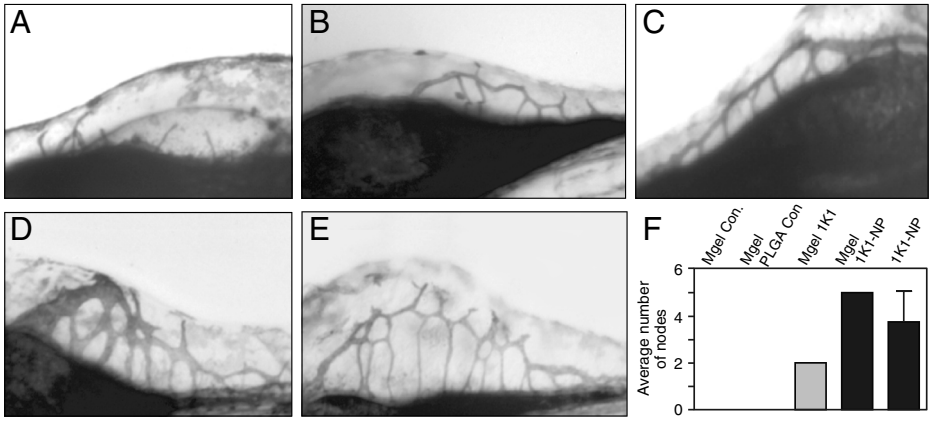

Fig. 5. Effect of 1K1 and 1K1-NP mediated angiogenesis in vivo using zebrafish model. 1K1 or 1K1-NP were injected with growth-factor-reduced matrigel (Mgel) near the subintestinal vessel. SIVs were then stained with alkaline phosphate and visualized in bright field. (*A*): vehicle (Mgel); (*B*) empty PLGA in Mgel (*C*) 1K1 in Mgel, (*D*) 1K1-NP in Mgel and (*E*) 1K1-NP. (*F*) Graph shows morphometric quantification of the effect of treatment on angiogenesis. Data shown mean SEM± from $n = 3$.

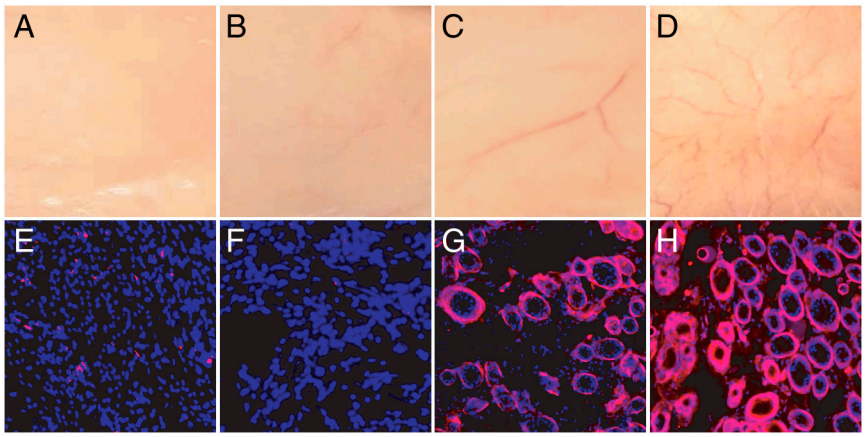

Fig. 6. Effect of 1K1 (200 ng/plug) and 1K1-NP (200 ng/plug) induced angiogenesis in growth-factor-reduced matrigel implants in vivo. *Upper* (*A–D*) shows gross morphology of the implants after everting the murine skin, and *Bottom* (*E–H*) shows cross sections where blood vessels are delineated with von Willebrand factor immunolabeling and appear *red*. Nuclei were counterstained with DAPI and appear *blue*. Images were captured at 512×512 pixels resolution. *A* and *E*: vehicle, *B* and *F*: empty NP, *C* and *G*: 1K1, *D* and *H*: 1K1 NP.

We and others have previously demonstrated that HGF/SF can mount a strong angiogenic response (12), both independently of other growth factors (10) and by inducing expression of VEGF (31). Furthermore, a study to assess the safety of intramuscular injection of HGF/SF plasmid to improve limb perfusion in patients with critical limb ischemia (the HGF-STAT trial) has recently revealed that intramuscular injection of HGF plasmid was safe and well tolerated, and limb tissue perfusion as measured by transcutaneous oxygen tension in patients with critical limb ischemia was found to have significantly improved at the highest doses used (32). These observations establish a strong clinical rationale to use HGF/SF in the management of ischemic diseases. However, the emerging hypothesis suggests that sustained release of angiogenic agents could be critical in defining the clinical outcome for therapeutic angiogenesis. In the present study, we demonstrate that a rationally engineered variant of HGF/SF can be integrated into a nanovector that alters the temporal presentation of the growth factor to the target cells, and thereby enhances the angiogenic outcome by modifying the downstream signaling cascade.

A key hurdle in translating growth factors to the clinics frequently lies in the heterogeneity of the polypeptide growth factor due to extensive protein glycosylation, which poses regulatory challenges for manufacturing. In the case of HGF/SF, additional challenges are the complex multidomain structure of the native protein that results in low production yields and a propensity of the protein to aggregate in physiological buffers. In this study, we investigated a truncated mutant of HGF/SF which can be expressed in high yields by yeast cells (unlike native HGF/SF), lacks glycosylation sequences and retains strong signaling activity. Next, we further improved the biological activity and therapeutic potential of 1K1 by incorporating the protein in nanoparticles from PLGA copolymer. While free 1K1 and 1K1-NP induced similar levels of ERK phosphorylation at early time points, we observed that the nanoparticle resulted in sustained activation of the MAPK signaling in contrast to free 1K1. In a previous study, the sustained activation of MAPK was reported to be critical for tubulogenesis while a transient activation was shown to be sufficient for the induction of cell proliferation (8, 24–25). This observation can possibly explain that while 1K1 and 1K1-NP exhibited similar levels of cell proliferation, the latter resulted in enhanced neovascularization in the in vivo matrigel implant and zebrafish angiogenesis assay. Excitingly, this observation also highlights the potential use of nanotechnology to temporally alter signaling pathways through controlled release thereby enable the dissection of distinct regulatory controls underlying biological phenomena. These results address the emerging paradigm that the sustained focal concentration of the active agent is critical for therapeutic angiogenesis, and may offer a robust strategy for the management of ischemic diseases.

Materials and Methods

Expression of 1K1 and HGF/SF. HGF/SF was produced from a derivative of the mouse myeloma cell line NS0 transfected with a full length HGF/SF cDNA. 1K1 was produced from a derivative of the yeast *Pichia pastoris* transfected with the 1K1 cDNA. Both proteins were purified from culture supernatants using Heparin-Sepharose chromatography followed by cation exchange chromatography on Mono S, yielding proteins >90% pure as judged by SDS gel electrophoresis.

Surface Plasmon Resonance Experiments. A fragment of the Met ectodomain corresponding to amino acids 25-567 (MET567) was used for immobilization on single flow cells of a CM5 chip equilibrated with 20 mM phosphate (pH 7.4), 150 mM NaCl, 50 μM EDTA, 0.005% Surfactant P20. The chip surface was first activated using the CM5 amine coupling immobilization method in the BIACore Control software (100 μL of 0.2 M 1-Ethyl-3-(3-dimethylaminopropyl)carbodiimide mixed with 100 μL 0.05 M N-hydroxysuccinimide to give reactive succinimide ester groups). Met567H was diluted in 10 mM sodium acetate at a final concentration of 400 nM and injected, until a ΔRU of ~1,500 was reached. Remaining active groups were blocked by injection of 70 μL of 1 M ethanolamine (pH 8.5). As a negative control, another flow cell of the CM5 chip was treated with the same program, but without protein. The chip was then reequilibrated with 10 mM Hepes, 150 mM NaCl, 3 mM EDTA, 0.005% Tween-20 (HBS-EP) (10 mM Hepes(pH 7.4), 150 mM NaCl,50 μM EDTA,0.005%Surfactant P20) + 0.2 mg/ml BSA and then a range of protein concentrations (diluted in HBS-EP + BSA) were injected at 20 μL/ min for 60 min followed by a 300 s dissociation time. The chip was regenerated using HBS-EP with 1 M NaCl.

Analytical Ultracentrifugation. Wild-type NK1, 1K1, and MET567 proteins were dialyzed against 25 mM phosphate, 150 mM NaCl, pH 7.4 prior to centrifugation. Measurements were made using a Beckman Optima XLA analytical ultracentrifuge using an intermediate speed sedimentation velocity method. Data were acquired in continuous mode analyzed using the program Sedfit in which the least-squares g(s*) sedimentation coefficient distribution is computed, where c is the concentration (in absorbance units), r is radius (in cm), t is time (in seconds), $c0$ is the loading concentration (in absorbance units), w is the angular velocity of the rotor (in radians/second) and r_m is the radius at the meniscus (in cm). Data were collected with incident light set at 278 nm. The g(s*) profiles were fitted with normal (Gaussian) distributions using ProFit, a nonlinear least-squares fitting package (Quantum Soft).

Engineering 1K1 Nanoparticle. 1K1 nanoparticles were made using the double emulsion/solvent extraction technique. Emulsion 1 was prepared using 50 mg PLGA (50:50) (MW 40–75 KDa) dissolved in 10 mL of acetonitrile. 104 ug 1K1 was encapsulated in 50 mg PLGA by sonication. Emulsion 2 was prepared using 0.5 g PVA (polyvinyl alcohol, Sigma, MW 9,000–10,000) and was dissolved in 9.3 mL of double distilled water and 0.7 mL of acetonitrile. An organic extraction buffer was made by dissolving 0.2 g PVA in 186 mL of double distilled water and 14 mL of acetonitrile. 1 mL of emulsion 2 was added to emulsion 1 and the solution was vortexed for ~1 min and was added to that organic buffer. This solution was stirred for 12 h to evaporate acetonitrile. This solution was centrifuged at 193,190 x 4 *g* (Sorvall Ultra Pro 80) for 1 h to pellet the nanoparticles, which was washed again with water and then characterized for size and morphology using a Nano-

zetasizer (Malvern) and transmission electron microscopy (TEM). The samples was spotted on copper grids and stained with uranyl acetate for TEM.

Cell Proliferation Assay. HUVECs were grown in 96 well plate and synchronized in 0.1% FBS prior to treatment with growth factors for 24, 48, or 72 h. Cells were treated with signal transduction inhibitors for 2 h prior to addition of growth factors. The percentage of viable cells was quantified with 3-(4, 5-Dimethylthiazol-2-yl)-5-(3-carboxymethoxyphenyl)-2-(4-sulfophenyl)-2H-tetrazolium (MTS) from the Cell Titer 96 Aqueous One Solution kit measured at 490 nm using a Versamax plate reader. Final absorbance, corresponding to cell proliferation, was plotted after subtracting background values from each data point.

HUVEC Tube Assay. HUVECs (25,000 cells per well) were seeded in a 96-well plate coated with growth-factor-reduced matrigel. Cells were treated with inhibitors for 2 h before adding the growth factors. After 8 h, images were taken under inverted light microscopy at 10× magnification (Nikon Eclipse).

Immunoblotting. HUVECs (70% confluent) were treated with 1K1, 1K1-NP, and HGF/SF (positive control) for 10 min and directly lysed in 3× loading buffer. The cells were pretreated with signal transduction inhibitors for at least 2 h before growth-factor treatment. Proteins were resolved on 10% SDS-PAGE gel. Membranes were probed for phosphorylated and total forms of MET, Akt, and Erk. Proteins were detected with horseradish peroxidase-conjugated anti-rabbit secondary antibodies and Lumi-LightPLUS Western Blotting Substrate (Roche Applied Science). The blots were developed using GeneSnap and optical density was quantified using Gene Tools (both from SynGene). Predetermined molecular weights standards were used as markers. Proteins were normalized against actin.

Zebrafish Angiogenesis Assay. Zebrafish (Tōbingen AB) (2 d post fertilization), were anesthetized in Tricaine (MESAB-ethyl-m-aminobenzoate methanesulphonate, 1% Na_2HPO_4, pH 7.0) and positioned on their side in a 1% agarose injection mold, and 9.2 nL of each sample was injected into the yolk sac next to the subintestinal vessel (SIV) using a Nanoject II injection device (Drummond Scientific). Zebrafish injected with growth-factor-reduced matrigel and 1 μM 1K1 as free or in nanoparticles were monitored for 24 and 48 h. Brightfield imaging was performed with a Nikon SMZ1500 stereomicroscope and a SPOT Flex camera.

in Vivo Matrigel Angiogenesis Assay in Mouse. Growth-factor-reduced matrigel (BD), mixed with growth factors were injected subcutaneously into balb/c mice. Mice were divided in two four groups: (A) vehicle control with growth-factor-reduced matrigel, (B) vehicle control with empty PLGA and growth-factor-reduced matrigel, (C) matrigel plug with 200 ng free 1K1 and (D) matrigel plug with 200 ng 1K1-NP. On day 12, gross response in the form of blood vessels formed (angiogenesis) was recorded with a high-resolution digital camera (Canon). The implants were excised and cryofrozen in optimal cutting temperature compound for immunohistochemistry.

Immunohistochemistry. The matrigel cryosections (18 μm) were fixed in −20 °C with ice cold methanol and probed overnight with primary rabbit antibody against von Willebrand factor (Dako) at 4 °C in blocking buffer. Samples were then probed with Alexa fluor 594 conjugated anti-rabbit secondary antibody at room temperature for 2 h. Nuclei were counterstained with DAPI. Images were captured with immunofluorescence microscope (Nikon Eclipse) at 10× magnification.

Statistical Analysis. Statistical significance was tested by using 1-way ANOVA followed by Dunnett's or Friedman's post hoc test. Bonferroni's test was used to test for overall dose-response effects (Graphical Prism 3 software). A value of $P < 0.05$ was considered significant.

ACKNOWLEDGMENTS. We thank Dr. Sudipta Basu, Sujan Kabir, and Nassim Kassam for useful discussions. E.G. is supported by Program Grants from United Kingdom Medical Research Council and the British Heart Foundation. S.Sengupta is supported by a Breast Cancer Research Program (BCRP) Era of Hope Scholar and BCRP Innovator Collaborative Award.

1. Rosamond W, et al. (2007) Heart disease and stroke statistics—2007 update: a report from the American Heart Association Statistics Committee and Stroke Statistics Subcommittee. *Circulation* 115:e69–e171.
2. Ferrara N, Kerbel RS (2005) Angiogenesis as a therapeutic target. *Nature* 438:967–974.
3. Kutryk MJB, et al. (2001) Angiogenesis: an emerging technology for the treatment of coronary artery disease. *Cardiology Rounds* VI:1–8.
4. Fortuin FD, et al. (2003) One-year follow-up of direct myocardial gene transfer of vascular endothelial growth factor-2 using naked plasmid deoxyribonucleic acid by way of thoracotomy in no-option patients. *Am J Cardiol* 92:436–439.
5. Simons M, et al. (2002) Pharmacological treatment of coronary artery disease with recombinant fibroblast growth factor-2. double-blind, randomized, controlled clinical trial. *Circulation* 105:793.
6. Yla-Herttuala S, et al. (2007) Vascular endothelial growth factors: biology and current status of clinical applications in cardiovascular medicine. *J Am Coll Cardiol* 49:1015–1026.
7. Gupta R, et al. (2009) Human studies of angiogenic gene therapy. *Cir Res* 105:724–736.
8. Zhou X, et al. (2008) Fibronectin fibrillogenesis regulates three dimensional neovessel formation. *Gene Dev* 22:1231–1243.
9. Borman S (2006) Glycosylation engineering. *Chem Eng News* 84:13–22.
10. Sengupta S, et al. (2003) Hepatocyte growth factor/scatter factor can induce angiogenesis independently of vascular endothelial growth factor. *Arterioscler Thromb Vasc Biol* 23:69–75.
11. Gherardi E, et al. (2006) Structural basis of hepatocyte growth factor/scatter factor and MET signaling. *Proc Nat'l Assoc Sci USA* 103:4046–4051.
12. Sengupta S, et al. (2003) Targeting of mitogen-activated protein kinases and phosphatidylinositol 3 kinase inhibits hepatocyte growth factor/scatter factor-induced angiogenesis. *Circulation* 107:2955–2961.
13. Ono K, et al. (1997) Enhanced expression of hepatocyte growth factor/c-Met by myocardial ischemia and reperfusion in a rat model. *Circulation* 95:2552–2558.
14. Schwall RH, et al. (1996) Heparin induces dimerization and confers proliferative activity onto the hepatocyte growth factor antagonists NK1 and NK2. *JCB* 133:709–718.
15. Chirgadze DY, et al. (1999) Crystal structure of the NK1 fragment of HGF/SF suggests a novel mode for growth factor dimerization and receptor binding. *Nat Struct Biol* 6:72–79.
16. Lietha D, et al. (2001) Crystal structures of NK1-heparin complexes reveal the basis for NK1 activity and enable engineering of potent agonists of the MET receptor. *EMBO J* 20:5543–5555.
17. Holmes O, et al. (2007) Insights into the structure/function of hepatocyte growth factor/scatter factor from studies with individual domains. *J Mol Biol* 367:395–408.
18. Sengupta S, et al. (2004) Nitric oxide modulates hepatocyte growth factor/scatter factor-induced angiogenesis. *Angiogenesis* 7:285–294.
19. Richardson TP, et al. (2001) Polymeric system for dual growth factor delivery. *Nat Biotechnol* 19:1029–1034.
20. Hsieh PCH, et al. (2006) Local controlled intramycardial delivery of platelet-derived growth factor improves postinfarction ventricular function without pulmonary toxicity. *Circulation* 114:637–644.
21. Kubo M, et al. (2009) Therapeutic neovascularization by nanotechnology-mediated cell- selective delivery of pitavastatin into the vascular endothelium. *Arterioscler Thromb Vasc Biol* 29:796–801.
22. Rocha FG, et al. (2008) The effect of sustained delivery of vascular endothelial growth factor on angiogenesis in tissue-engineered intestine. *Biomaterials* 29:2884–2890.
23. Chappell JC, et al. (2008) Targeted delivery of nanoparticles bearing fibroblast growth factor-2 by ultrasonic microbubble destruction for therapeutic arteriogenesis. *Small* 4:1769–1777.
24. Karihaloo A, et al. (2004) Hepatocyte growth factor-mediated renal epithelial branching morphogenesis is regulated by glypican-4 expression. *Mol Cell Biol* 24:8745–8752.
25. Rosario M, Birchmeier W (2003) How to make tubes: signaling by the Met receptor tyrosine kinase. *Trends Cell Biol* 13:328–335.
26. Stoletov K, et al. (2007) High-resolution imaging of the dynamic tumor cell-vascular interface in transparent zebrafish. *Proc Natl Acad Sci USA* 104:17406–17411.
27. Ny A, et al. (2006) Zebrafish and Xenops tadpoles: small animal models to study angiogenesis and lymphangiogenesis. *Exp Cell Res* 312:684–693.
28. Wang N, et al. (2009) Effect of hepatocyte growth-promoting factors on myocardial ischemia during exercise in patients with severe coronary artery disease. *Int Heart J* 50:291–299.
29. Laham RJ, et al. (2001) Gene transfer for angiogenesis in coronary artery disease. *Annual Rev Med* 52:485–502.
30. Jin H, et al. (2003) Early treatment with hepatocyte growth factor improves cardiac function in experimental heart failure induced by myocardial infarction. *The Journal of Pharmacology and Experimental Therapeutics* 304:654–660.
31. Van Belle E, et al. (1998) Potentiated angiogenic effect of scatter factor/hepatocyte growth factor via induction of vascular endothelial growth factor: the case for paracrine amplification of angiogenesis. *Circulation* 97:381–390.
32. Powell RJ, et al. (2008) Results of a double-blind, placebo-controlled study to assess the safety of intramuscular injection of hepatocyte growth factor plasmid to improve limb perfusion in patients with critical limb ischemia. *Circulation* 118:58–65.